Molecular Dynamics Study of Droplet Impinging/Freezing on Cold Surface

Moromisato, Shu
Graduate School of Engineering, Kyushu Institute of Technology

Hsiu-Yang Tseng
Department of Mechanical Engineering, National Taiwan University of Science and Technology

Nagayama, Gyoko
Department of Mechanical Engineering, Kyushu Institute of Technology

https://doi.org/10.5109/7323353

出版情報：Proceedings of International Exchange and Innovation Conference on Engineering & Sciences (IEICES). 10, pp.805-811, 2024-10-17. International Exchange and Innovation Conference on Engineering & Sciences
バージョン：

Molecular dynamics study of droplet impinging/freezing on cold surface.

Shu Moromisato[1], Hsiu-Yang Tseng[2], Gyoko Nagayama[3]
[1]Graduate School of Engineering, Kyushu Institute of Technology, Kitakyushu, Fukuoka 804-8550, Japan
[2]Department of Mechanical Engineering, National Taiwan University of Science and Technology, Taipei 106, Taiwan
[3]Department of Mechanical Engineering, Kyushu Institute of Technology, Kitakyushu, Fukuoka 804-8550, Japan
Corresponding author email: nagayama.gyoko725@mail.kyutech.jp

Abstract: *Rapid freezing is utilized for cell preservation without the application of cryoprotectants to rapidly freeze water-containing specimens such as living organisms, foods, and paints. Prior studies have predominantly focused on the freezing behavior of micrometer-to-millimeter-sized droplets on cold surfaces, examining variables such as droplet shape and freezing time. However, the freezing dynamics of nanometer-sized droplets on cold surfaces remain unexplored. In this study, we employed molecular dynamics (MD) simulations to investigate the freezing behavior of nanometer-sized droplets impacting a cold surface. We did not observe a corner forming at the top of the nanometer-sized droplets because the freezing process was too rapid for internal flow to develop. Our findings indicate that the droplet's temperature rapidly increases due to the heat of adsorption upon contact with the surface and the conversion of kinetic energy. Furthermore, we found that the contact angle post-freezing is influenced by multiple factors, including wettability, temperature of cold surface, impact speed, and droplet size.*

Keywords: Molecular Dynamics Simulation; Impinging; Freezing; Droplet; Water

1. INTRODUCTION

Droplet freezing has adverse effects not only in natural environment [1], but also on infrastructure like airplanes and power lines [2-8]. In wind turbines, frozen droplets lead to power loss and control errors, as well as mechanical and electrical faults that can compromise the safe operation of the turbines [5]. Ice accumulation on electrical wires can cause failures. The weight of the ice coating does not damage the electric cables, but the wind moving against the ice coating causes the wires to shake violently. When the ice falls from the wires, the cables rebound significantly, potentially leading to short-circuit accidents [6]. In aircrafts, ice coating alters the shape of the wings, reducing lift and increasing drag. When the attached ice peels off, it can damage the airframe. Uneven distribution of ice can also cause differences in lift and drag between the left and right sides of the airframe, leading to instability and potentially fatal accidents [7-8]. As ice coating adversely affects many products, numerous studies have focused on droplet freezing and methods to prevent ice accumulation [9-10]. Freezing has also been used for cell preservation [11]. Traditional cell cryopreservation involves vitrifying both the water inside and outside cells using preservatives. However, this method may have adverse effect on the cells. Recently, some research has developed a technique to cryopreserve cells by ejecting cell-laden droplets from an inkjet printer onto a cold substrate. This method has succeeded in vitrifying and preserving the water inside and outside the cells without using any preservatives [12].

Studies on the freezing of droplets on cold surface has been conducted using both experimental and simulation approaches. In their experiment, Wang et al. [13] conducted an experiment in which a 750 μm-diameter droplet was dropped onto a copper substrate at room temperature or a low temperature, followed by the droplet's freezing by lowering the temperature of cold surface. When the experiment was conducted with water, the freezing front began near the cold surface and progressed towards the top of the droplet. Additionally, a corner formed at the top of the droplet just before it was completely frozen. This corner became more pronounced as the temperature of cold surface decreased. In contrast, when the experiment was conducted with peanut oil, no corner formed at the top of the droplet when it was fully frozen. Schremb et al. [14] pinched a 2 to 5 mm-diameter droplet between glass substrates and observed the interior of the droplet during freezing by lowering the temperature. They distinguished the freezing process into two stages. In the first stage, freezing started with a mixture of liquid and solid, and in the second stage, the remaining liquid was also quenched. They concluded that a corner formed in the freezing droplet during the second stage due to the density difference generated. The volume expansion during freezing was a result of the density difference between the solid and liquid, which also caused internal convection within the droplet due to the fixed three-phase contact line. Chang et al. [15] conducted a study to investigate the effects of wettability and impact speed on the freezing process of a 2.67 mm-diameter droplet on a hydrophilic substrate and a superhydrophobic substrate. They divided the process into four stages based on the time variation of the droplet temperature. The first stage involved the droplet cooling and the temperature decreasing. The second stage involved the release of latent heat from the formation of crystal nuclei, causing the temperature to increase. The third stage involved the temperature starting to decrease again. The fourth stage involved the formation of a corner at the top of the droplet and the droplet being covered with frost. For the hydrophilic substrate, they found that when the impact speed was low, freezing was completed before the droplet could completely spread. When the impact speed was high, the droplet shape was similar to that of a droplet placed on a hydrophilic substrate at room temperature. On the other hand, for the superhydrophobic substrate, there was no relationship between the impact speed and the droplet shape during freezing. Additionally, there was a correlation between the impact speed and the freezing time. The freezing time shortened as the

temperature of cold surface decreased, but the superhydrophobic substrate showed a sharper decrease in freezing time compared to the hydrophilic substrate. Artur et al. [16] formed a layer of organic matter on a surface and froze a 3 mm droplet on it. They found that the freezing time varied depending on the thickness of the organic matter layer. The results revealed that the time it took for the droplet to freeze varied according to the thickness of the organic matter layer. This difference in freezing time was attributed not only to variations in contact angles that led to differences in contact areas but also to the presence of the organic matter layer itself. In simulations, several attempts have been made to theoretically reproduce droplet freezing [12-13, 15-16]. Chaudhary et al. [17] conducted a study on the effect of wettability on droplet freezing. They employed numerical solutions of the heat conduction equation to analyze the temperature distribution at the time of nucleation. Their findings revealed that the temperature distribution was non-uniform; droplets that were farther from the cold surface exhibited a greater decrease in temperature after nucleation. This phenomenon was more pronounced on hydrophobic substrates than on hydrophilic ones. Additionally, they found that the isotherms were initially parallel to the cold surface at the beginning of freezing. But it became concave as freezing progressed. Mirabedin et al. [18] carried out a numerical analysis of freezing, taking into account evaporation for droplets with diameters ranging from 200 to 900 μm. They examined the effects of the initial temperature of the droplet and the droplet diameters on freezing. The findings indicated that the evaporation flux had a more significant impact on freezing than convection and radiation. Moreover, if evaporation was not considered, a high initial temperature prolonged the freezing time. However, when evaporation was factored in, a high initial temperature resulted in increased evaporation flux, leading to faster freezing. The study also revealed that larger droplet diameters resulted in longer freezing times, and this trend remained consistent, regardless of the presence or absence of evaporation.

Previous research has focused on droplets with diameters ranging from millimeters to micrometers. However, the freezing behavior of nanometer-sized droplets remains largely unexplored. This may be because these small droplets evaporate before adhering to the substrate. Molecular dynamics simulations allow for the observation of the movement of each atom, making them suitable for studying nanometer-sized droplets [19]. In this study, molecular dynamics simulations were used to simulate the impact of droplet on cold surface. The simulation results revealed that the freezing behavior of nanometer-sized droplets differs from that of larger droplets in previous studies mentioned here. Specifically, no corners were generated at the top of the droplet, and the contact angle after freezing varied with factors such as wettability, impact speed, and temperature of cold surface. Additionally, the freezing behavior changed as the droplet size changed, and a three-step freezing process was observed for a droplet with 10,000 molecules. Upon contact with the cold surface, the temperature of the droplet increased due to the heat of adsorption and the kinetic energy from the impact velocity.

2. METHOD

We utilized molecular dynamics simulations to investigate the freezing behavior of water droplets upon impact with a silicon substrate. All simulations were performed using the LAMMPS (Large-scale Atomic/Molecular Massively Parallel Simulator) software package [20]. The simulation results were processed and visualized using OVITO (the Open Visualization Tool) [21].

The system comprises a substrate and a droplet. The substrate is 0.9 nm in thickness, consisting of silicon atoms arranged in a diamond structure with a lattice constant of 0.54307 nm. The initial configuration of the droplet is a rectangular parallelepiped containing 1000 to 10,000 water molecules, positioned initially 1 to 5 nm away from the cold surface.

The molecular interaction of water-water is simulated using the TIP4P/Ice model [22], a four-site rigid body model with charges at each point and dummy charges. The potential of TIP4P/Ice model is shown below, with a Coulomb term adding to the Lennard-Jones potential [23].

$$U_{ij} = 4\varepsilon_{ij}\left[\left(\frac{\sigma_{ij}}{r_{ij}}\right)^{12} - \left(\frac{\sigma_{ij}}{r_{ij}}\right)^{6}\right] + \frac{cq_iq_j}{4\pi\varepsilon_0 r_{ij}} \quad (1)$$

Here r_{ij} is the distance between two atoms i and j, ε_{ij} is the well depth of the potential, and σ_{ij} is the atomic diameter, c is the energy conversion constant, q_i, q_j are the atomic charges, and ε_0 is the vacuum dielectric constant. The parameters of the TIP4P/Ice model are detailed in Table 1. The SHAKE algorithm fixes the oxygen-hydrogen bonds and angles. The PPPM (Particle-particle-particle-mesh) method is used to calculate the long-range Coulomb action with an accuracy of 10^{-5}.

Table 1. Parameters of TIP4P/Ice model [22].

q_O [e]	q_H [e]	r_{OH} [nm]	θ_{HOH} [degree]
−1.1794	0.5897	0.09572	104.52

Stillinger-Weber potential [24] was used to calculate the silicon-silicon interaction. To calculate the interactions between silicon-water, the modified Lennard-Jones potential was used based on the Lorentz-Berthelot mixing rules [25], [26]:

$$U_{ij} = 4\varepsilon_{ij}{}'\left[\left(\frac{\sigma_{ij}}{r_{ij}}\right)^{12} - \left(\frac{\sigma_{ij}}{r_{ij}}\right)^{6}\right] \quad (2)$$

$$\varepsilon_{ij}{}' = \alpha\sqrt{\varepsilon_i \cdot \varepsilon_j} \quad (3)$$

The energy parameter ε is tuned by a parameter α to represent different surface wettability between the substrate and the droplet. Increasing α enhances the potential well depth, stabilizing particles at lower potentials and reinforcing interparticle bonds, resulting in increased hydrophilicity.

Fig. 1 shows a snapshot of the initial state. The simulation box dimensions are 16.7 nm in the x and y directions and 21.7 nm in the z direction. Periodic boundary conditions are implemented in the x and y directions, while specular boundary conditions are utilized in the z direction. The bottom layer of the substrate is fixed by setting the acting force to zero. To control the initial droplet temperature at 300 K and vary the temperature of cold surface from 100 to 260 K, the canonical ensemble is employed. The

Velocity Verlet algorithm is utilized to solve the equations of motion with a time step of 0.5 fs.
The droplet and substrate are initially positioned and equilibrated using the canonical ensemble for 0.25 ns. Following equilibration, the droplet and a section of the substrate were simulated under the microcanonical ensemble, while the temperature of cold surface control layer was maintained using the canonical ensemble. To commence the impingement process, the droplet is imparted with a velocity directed towards the substrate and simulate for 0.75 ns to collect data.

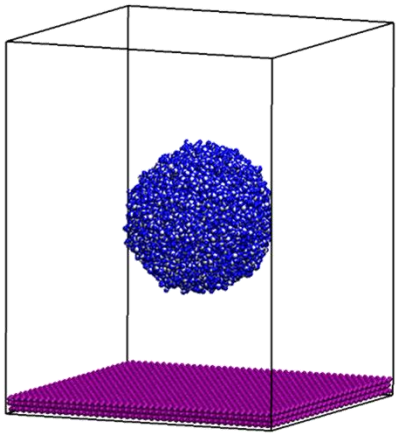

Fig. 1. Initial state of simulation system.

In this study, the wettability is assessed using the contact angle at 300 K. Given the insignificant influence of gravity on nanometer-sized droplets when compared to surface tension, the effect of gravity is disregarded in molecular dynamics simulations, and the contact angle θ is calculated using the θ/2 method [27]. We measure the contact radius and droplet height from the density distribution. The values of α along with the contact angles employed in this study, are presented in Table 3. Fig. 2 shows snapshots at 300 K for each wettability. The simulations investigate the impact of wettability on freezing across a spectrum ranging from hydrophilic (θ = 0 degrees) to hydrophobic (θ = 110 degrees).

Table 3. Potential parameter α and contact angles.

Cases	α	θ [degree]
Case 1	1	0
Case 2	0.5	0
Case 3	0.1	110

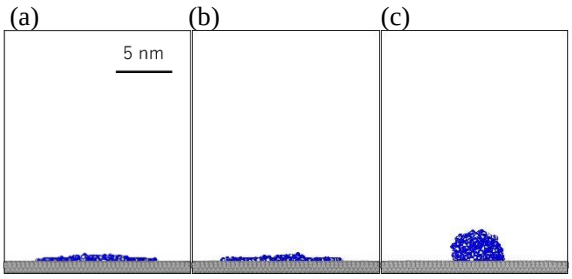

Fig. 2. Droplet on a solid surface at 300 K (a) case 1 of $\alpha = 1$, (b) case 2 of $\alpha = 0.5$, (c) case 3 of $\alpha = 0.1$.

The contact angle after freezing (freezing angle) is evaluated as shown in Fig. 3 using the curve fitting method of ImageJ [28]. This approach was selected due to the non-smooth density distribution following freezing, making it infeasible to calculate the contact radius and droplet height using the conventional technique employed for droplets at 300 K. As the shape of the droplets remain unaltered after freezing, the contact angle is measured from a static image.

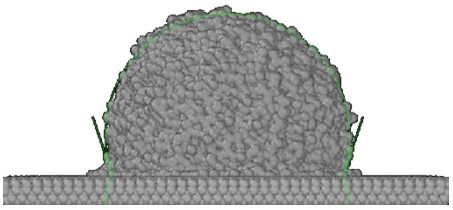

Fig. 3. Freezing angle measured after an impinging droplet frozen on the cold surface.

3. RESULT AND DISCUSSION

3.1 The shape of the droplet

In previous studies, the angle at the top of the micrometer to millimeter-sized droplets during freezing was significantly influenced by temperature of cold surface. Therefore, this study conducted simulations using 10,000 molecules, an impact velocity of 10 m/s, a hydrophilic surface with α = 1 wettability, and temperatures of cold surface of 100 K, 200 K, and 260 K to determine if a corner forms during droplet freezing. The results of these simulations are illustrated in Fig. 4, which displays screenshots from the different temperature of cold surface simulations. The simulations were run for enough steps, and the frozen droplet is displayed in each screenshot.

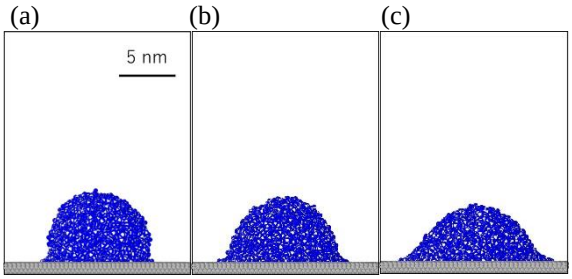

Fig. 4. Frozen droplets on cold surface at different temperatures: (a) T=100 K, (b)T=200 K, (c)T=260 K.

Droplet freezing was simulated at three different temperatures of cold surface, and in each instance, a freezing corner failed to form at the droplet's top. Previous studies have reported that a corner typically forms at the top of a droplet upon freezing on a substrate. For micrometer to millimeter-sized droplets in these studies, internal flows induced by density and surface tension differences during freezing resulted in the formation of a corner at the droplet's top [14-15]. However, it is hypothesized that the nanometer-sized droplets studied here froze too quickly for such internal flows to occur, thereby preventing the formation of a corner at the top. Consequently, no corner was observed at the top of the droplets in this study.

3.2 Influence temperature of cold surface, particle number, impact speed, and wettability on freezing angle

Fig. 5 illustrates the impact of varying the temperature of cold surface on the freezing angle. In this scenario, the particle number is set at 10,000, the impact speed at 10 m/s, and the surface is hydrophilic with a value of $\alpha = 1$. The data demonstrates that the freezing angle diminishes as the temperature of cold surface rises. Specifically, the freezing angle at 260 K is approximately 40% lower than that at 100 K. Furthermore, when the temperature of cold surface is 200 K or below, the droplet shape resembles that of a hydrophobic surface, even if the contact angle at 300 K is 0. At 200 K or below, it appears that the freezing angle is significantly affected due to the freezing rate being much faster than the spreading rate.

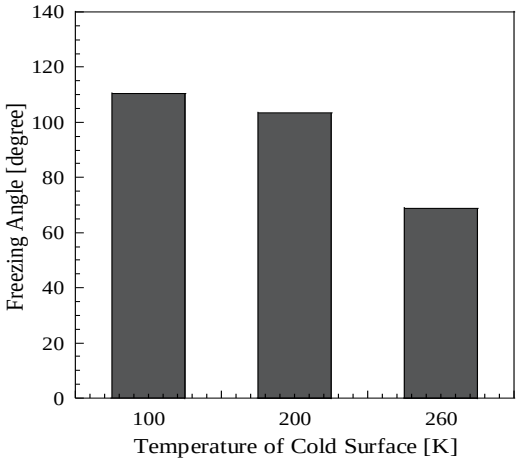

Fig. 5. Freezing angle of droplet on cold surface at different temperatures.

In Fig. 6, we compare the freezing angles of droplets containing 1,000 and 10,000 molecules at each temperature of cold surface. The freezing angle of a droplet with 1,000 molecules does not surpass 90 degrees, even at a temperature of cold surface of 100 K. Therefore, the freezing behavior is different for droplets with 1,000 and 10,000 molecules. Fig. 7 and 8 depict snapshots of the freezing process for droplets with 1,000 and 10,000 molecules, respectively. These images reveal the reasons behind the similar freezing angles for droplets with 10,000 molecules and those on hydrophobic surfaces. This is due to the freezing behavior of the droplet. For droplets with 1,000 molecules, after colliding with the cld surface (as shown in Fig. 7(b)), the droplet wets and spreads on the surface before freezing (as shown in Fig. 7(c)). In contrast, for droplets with 10,000 molecules, after colliding with the surface (as shown in Fig. 8(b)), the lower part of the droplet freezes upon contact with the surface (as shown in Fig. 8(c)). Then, the upper part of the droplet lands on the frozen lower part (as shown in Fig. 8(d)). The upper part is cooled by heat conduction through the lower part of the droplet (as shown in Fig. 8(e)). As a result, it does not wet and spread like droplets with 1,000 molecules. It undergoes a three-stage freezing process and eventually freezes into a shape similar to that of a droplet on a hydrophobic surface.

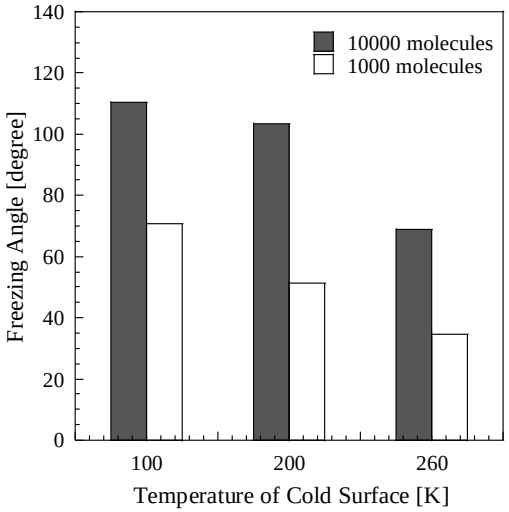

Fig. 6. Freezing angle of droplet with different size.

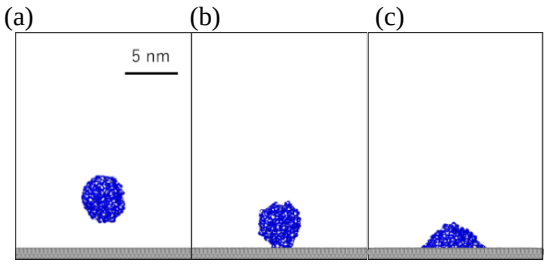

Fig. 7. Freezing process of impinging droplet with 1000 molecules: (a) 0 ps, (b) 235 ps, (c) 275 ps.

The temperature distribution of a droplet with 10,000 molecules was recorded and visualized. The temperature distribution of the droplet from the start of the simulation to 250 ps is shown in Fig. 9. Fig. 9(a) shows the temperature distribution at the start of the simulation. In Fig. 9(b), when the droplet makes contact with the surface, a temperature rise (yellow part) is observed at the portion of the droplet that adheres. Fig. 10 presents the temperature distribution in the z direction. This graph also shows that the temperature rises near the surface. Fig. 11(a) shows the time variation of droplet temperature at an impact velocity of 10 m/s, while Fig. 11(b) shows the time variation of droplet temperature at an impact velocity of 0 m/s. As depicted in Fig. 11, the temperature rise occurs upon contact between the droplet and the substrate. The findings illustrated in Fig. 11 indicate that the difference in enthalpy and the introduction of impact velocity led to a rise in temperature, as evidenced by the highest temperatures of 312.109 K in Fig. 11(a) and 309.308 K in Fig. 11(b). Fig. 12 illustrates the variation in temperature rise of a droplet upon substrate impact, as the impact velocity is altered. The chart depicts that the heat generated surpasses the heat of adsorption when impact velocity is taken into account.

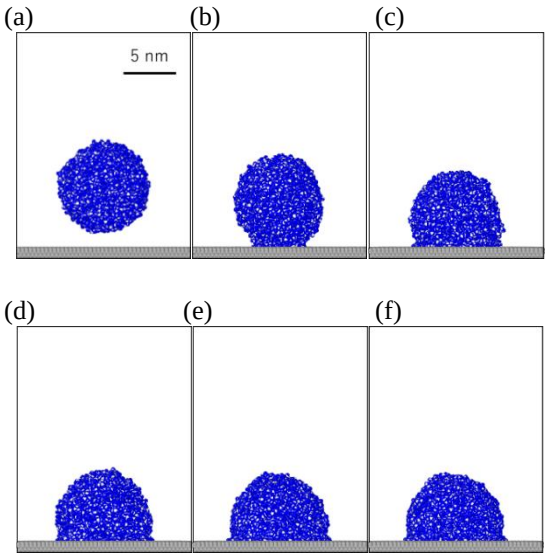

Fig. 8. Freezing process of impinging droplet with 10000 molecules: (a) 0 ps, (b) 100 ps, (c) 125 ps, (d) 145 ps, (e) 205 ps, (f) 250 ps.

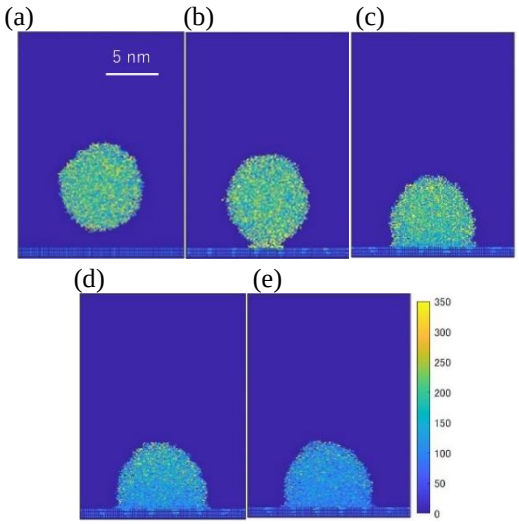

Fig. 9. Temporal temperature distribution at (a) 0 ps, (b) 100 ps, (c) 135 ps, (d) 205 ps, (d) 250 ps.

Additionally, the data reveals that as the impact velocity rises, the droplet temperature increases, suggesting that the kinetic energy is transformed into droplet temperature upon impact with the substrate. After the droplet is completely adsorbed on the substrate (as shown Fig. 9(c)), the color of the droplet changes from yellow to blue. This transformation occurs as a result of heat transfer from the droplet, which has a higher temperature, to the substrate, which has a lower temperature. At the beginning of the droplet freezing, the temperature of the portion close to the substrate decreases (as shown Fig. 9(d)). Subsequently, the cooling process propagates from the middle portion of the droplet to the upper portion (as shown Fig. 9(e)). Thus, the freezing process comprises three distinct stages: (1) temperature rise upon contact with surface, (2) a decrease in temperature at the lower portion of the droplet, and (3) cooling of the upper portion of the droplet through the already cooled lower portion. Consequently, the freezing angle becomes similar to that of a droplet on a hydrophobic surface with a droplet count of 10,000 molecules.

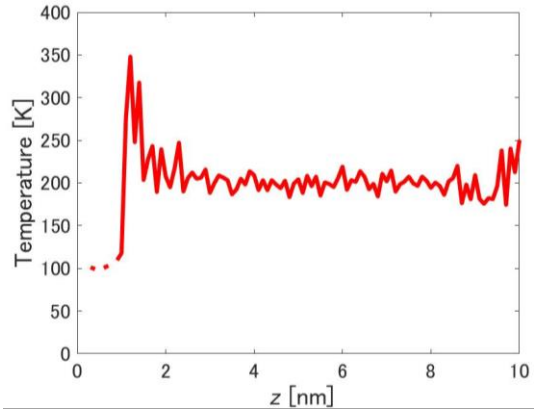

Fig. 10. Temperature distribution in the *z* direction.

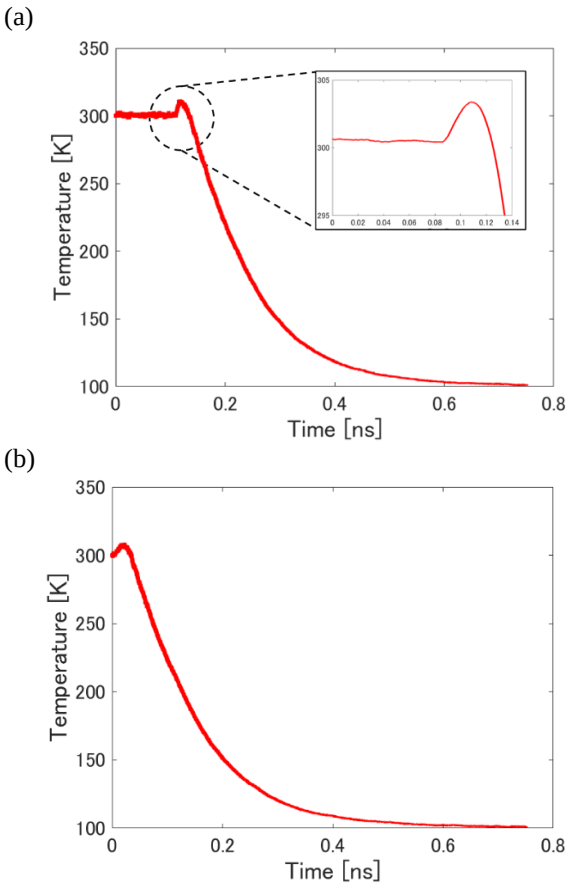

Fig. 11. Temporal evolution of droplet temperature with initial impact velocity of (a) 10 m/s, (b) 0 m/s.

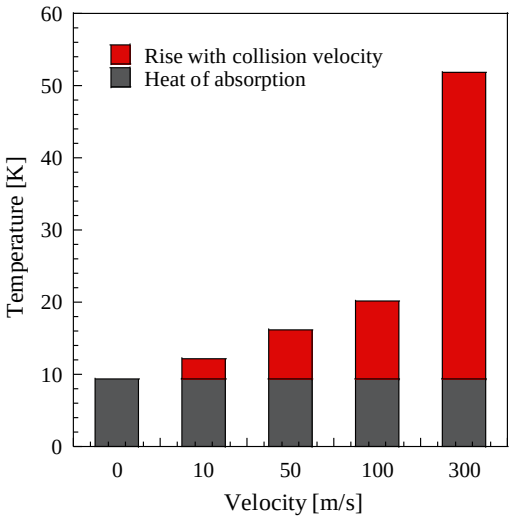

Fig. 12. Droplet temperature at the moment of drop contacting surface.

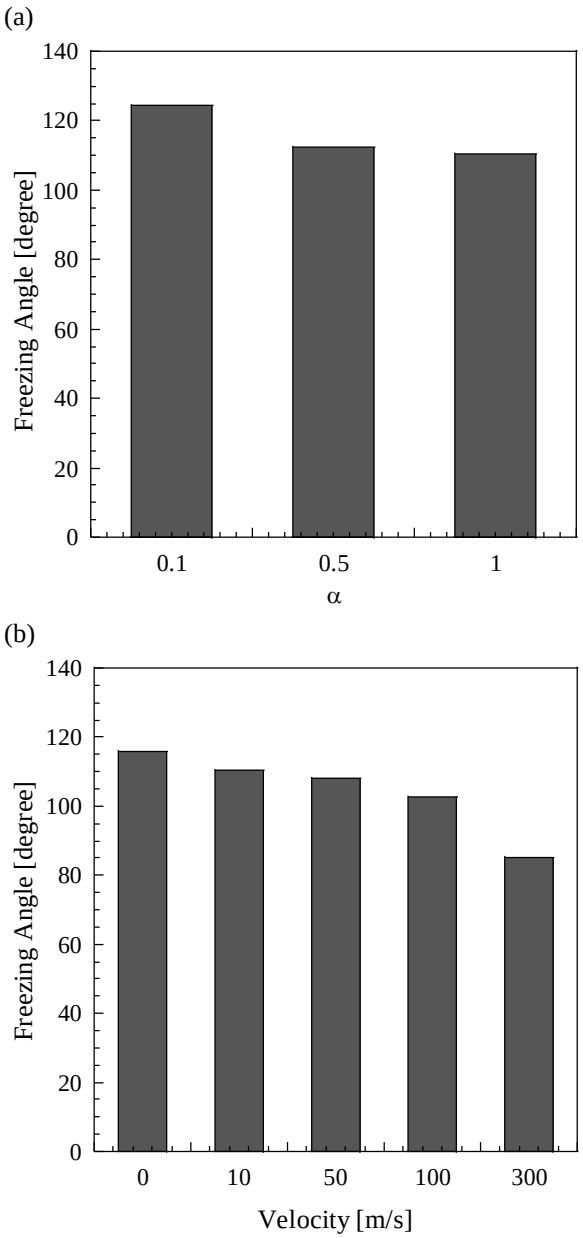

Fig. 13. (a) Freezing angle versus wettability, (b) freezing angle versus impact velocity.

The present research focused on examining the consequences of wettability and impact velocity on the freezing angle. Fig. 13(a) demonstrates the freezing angle when wettability was manipulated, while Fig. 13(b) shows the freezing angle when the impact speed was altered. In both cases, the particle number was set at 10,000, with a impact speed of 10 m/s and a temperature of cold surface of 100 K in Fig. 13 (a), and a hydrophilic surface with $\alpha = 1$ and a temperature of cold surface of 100 K in Fig. 13 (b). As the value of α decreases, the wettability becomes more hydrophobic. As shown in Fig. 13(a), the freezing angle tends to rise as the wettability becomes more hydrophobic. On the other hand, from Fig. 13(b), the freezing angle tends to decrease as the impact speed increases. These trends are similar to those observed in previous experimental study [15].

4. CONCLUSION

We explored the freezing behavior of a water droplet on a cold surface using MD simulations with LAMMPS. The simulation results showed that the droplet did not form a corner at the top during freezing. This phenomenon was attributed to the absence of convective flow inside the droplet, which was due to the rapid freezing of the nanometer-sized droplet. It was observed that the freezing angle tended to decrease as the temperature of cold surface increased. When the temperature of cold surface was below 200 K, the droplet shape resembled that of a hydrophobic substrate. Comparing the freezing behavior of droplets with 1000 molecules to those with 10,000 molecules, it was found that freezing occurred in three stages for droplets with 10,000 molecules. The temperature distribution images, and droplet temperature graphs depicted the temperature rise occasioned by the heat of adsorption and the impact velocity at the point of impact. As the impact velocity increased, the freezing angle decreased. Additionally, improved wettability resulted in an increased freezing angle.

Acknowledgments

This work was supported by the Ministry of Education, Science and Culture of the Japanese Government through the Grant-in-Aid for Scientific Research, Project No. 22K18773 & 22H01416, the research supercomputing services by the Research Institute for Information Technology, Kyushu University, and Osaka University.

5. REFERENCES

[1] Michael P. Fuller, Andrew M. Fuller, Spyridon Kaniouras, Jack Christophers, Troy Fredericks, The freezing characteristics of wheat at ear emergence, European Journal of Agronomy, vol. 26, no. 4, pp. 435-441, 2007.

[2] Linyue Gao, Hui Hu, Wind turbine icing characteristics and icing-induced power losses to utility-scale wind turbines, Proceedings of the National Academy of Sciences, vol. 118, no. 42, 2021.

[3] Frank T. Lynch, Abdollah Khodadoust, Effects of ice accretions on aircraft aerodynamics, Progress in Aerospace Sciences, vol. 37, pp. 669-767, 2001.

[4] Zihan Zhou, Yanjun Shen, Jianshuai Hao, Zhipeng Bai, Yuting Liu, Haibo Kou, Inexpensive anti-icing concrete material for application to tunnel and slope engineering infrastructures in cold regions, ACS Applied Materials & Interfaces, vol. 13, no. 44, pp. 53030-53045, 2021.

[5] Olivier Parent, Adrian Ilinca, Anti-icing and de-icing techniques for wind turbines: critical review, Cold Regions Science and Technology, vol. 65, no. 1, pp. 88-96, 2011.

[6] C. Volat, M. Farzaneh, De-icing/anti-icing techniques for oower lines: current methods and future direction, engineering, Environmental Science, 2005.

[7] Mark G. Potapczuk, Aircraft Icing Research at NASA Glenn Research Center, Journal of Aerospace Engineering, vol. 26, no. 2, 2013.

[8] Frank T. Lyncha, Abdollah Khodadoust, Effects of ice accretions on aircraft aerodynamics, Progress in Aerospace Sciences, vol. 37, pp. 669-767, 2001.

[9] Zdobyslaw Goraj, An overview of the deicing and antiicing technologies with prospects for the future, 24th International Congress of the Aeronautical Sciences, 2004.

[10] František Mikší, Jan Skolil, Josef Kotlík, Josef Čáslavský, Takahiko Miyazaki, Shigeru Koyma, Helena Půčková, Petr Levek, Antifreeze heat transfer fluid based on propane-1,3-diole, Proceedings of International Exchange and Innovation Conference on Engineering & Sciences, vol. 3, pp. 117-120, 2017.

[11] Chiu-Jen Chen, Min-Heng Kao, Noel A. S. Alvarado, Yong-Ming Ye, Hsiu-Yang Tseng, Microfluidic determination of distinct membrane transport properties between lung adenocarcinoma cells cl1-0, Biosensors, vol. 12, no. 4, 2022.

[12] Yoshitake Akiyama, Masato Shinosea, Hiroki Watanabea, Shigeru Yamadab, Yasunari Kanda, Cryoprotectant-free cryopreservation of mammalian cells by superflash freezing, Proceedings of the National Academy of Sciences, vol. 116, no. 16, 2019.

[13] Wang Jieteng, Liu Zhongliang, Gou Yujun, Zhang Xinhua, Cheng Shuiyuan, Deformation of freezing water droplets on a cold copper surface, Science in China Series E: Technological Sciences, vol. 49, no. 5, pp. 590-600, 2006.

[14] Markus Schremb, Cameron Tropea, Solidification of supercooled water in the vicinity of a solid wall, Physical Review E, vol. 94, no. 5, 2016.

[15] Shinan Chang, Haifeng Qi, Shu Zhou, Yinglin Yang, Experimental and numerical study on freezing process of water droplets under surfaces with different wettability, Applied Thermal Engineering, vol. 219, 2023.

[16] Emil Korczeniewski, Paweł Bryk, Stanisław Koter, Piotr Kowalczyk, Wojciech Kujawski, Joanna Kujawa, and Artur P. Terzyk, Revisiting wetting, freezing, and evaporation mechanisms of water on copper, ACS Applied Materials & Interfaces, vol. 13, no. 31, pp. 37893–37903, 2021.

[17] Gaurav Chaudhary, Ri Li, Freezing of water droplets on solid surfaces: An experimental and numerical study, Experimental Thermal and Fluid Science, vol. 57, pp. 86-93, 2014.

[18] Seyed Milad Mirabedin, Fatola Farhad, Numerical investigation of solidification of single droplets with and without evaporation mechanism, ScienceDirect, vol. 73, pp. 219-225, 2017.

[19] M. Khalid Hossain, M. Ishak Khan, T. Sarkar Akash, Kenichi Hashizume, Molecular dynamics simulation for barium zirconate proton conducting oxide energy materials: a mini review, Proceeding of International Exchange and Innovation Conference on Engineering & Sciences, vol. 7, pp. 1-6, 2021.

[20] Aidan P. Thompson, H. Metin Aktulga, Richard Berger, Dan S. Bolintineanu, W. Michael Brown, Paul S. Crozier, Pieter J. in 't Veld, Axel Kohlmeyer, Stan G. Moore , Trung Dac Nguyen, Ray Shan, Mark J. Stevens, Julien Tranchida, Christian Trott, Steven J. Plimpton, LAMMPS - a flexible simulation tool for particle-based materials modeling at the atomic, meso, and continuum scales, Computer Physics Communications, vol. 271, 2022.

[21] Alexander Stukowski, Visualization and analysis of atomistic simulation data with OVITO–the open visualization tool, Modeling and Simulation in Materials Science and Engineering, vol. 18, 2010.

[22] J. L. F. Abascal, E. Sanz, R. García Fernández, C. Vega, A potential model for the study of ices and amorphous water: TIP4P/Ice, Journal of Chemical Physics, vol. 122, no. 23, 2005.

[23] J. E. Jones, Sydney Chapman, On the determination of molecular fields. -I. from the variation of the viscosity of a gas with temperature, Proceedings of the Royal Society of London, vol. 106, no. 738, pp. 441-462, 1924.

[24] Frank H. Stillinger, Thomas A, Computer simulation of local order in condensed phases of silicon, Physical Review B, vol. 31, no. 8, pp. 5262-5271, 1985.

[25] H. A. Lorentz, Ueber die anwendung des satzes vom virial in der kinetischen theorie der gase, Annalen der Physik, vol. 248, no. 1, pp. 127-136, 1881.

[26] Daniel Berthelot, Sur le mélange des gaz, Comptes Rendus Hebdomadaires des Séances de l'Académie des Sciences, vol. 126, pp. 1703-1706, 1898.

[27] Gyoko Nagayama, Dejian Zhang, Intermediate wetting state at nano/microstructured surfaces, Soft Matter, vol. 16, pp. 3514-3521, 2020.

[28] A.F. Stalder, G. Kulik, D. Sage, L. Barbieri, P. Hoffmann, A snake-based approach to accurate determination of both contact points and contact angle, Colloids and Surfaces A: Physicochemical and Engineering Aspects, Vol. 286, no. 1–3, pp. 92-103 2006.